STRAINED ISLAND FORMATION IN HETEROEPITAXY

LEE Chun Kin

M. PHIL.

THE HONG KONG POLYTECHNIC UNIVERSITY

2002

Acknowledgments

I would like to take this opportunity to express my sincere gratitude to my supervisor Dr. C. H. Lam for his invaluable guidance, support and encouragement throughout the years. I would like to thank Prof. L. M. Sander of the University of Michigan for his advice. It is my pleasure to thank Prof. B. G. Orr and Prof. F. G. Shin for helpful comments. Special thanks are due to Mr. T. L. Chan and Mr. M. K. Lee for their technical support of the computer cluster. Finally, I would like to acknowledge Dr. Terence Lo of the Department of English for his suggestions regarding the use of English and content organization of this thesis.

Abstract

Morphological evolution of strained heteroepitaxial films is studied using large scale kinetic Monte Carlo simulations in 1+1 dimensions. Films and substrates are modeled by square lattices of balls and springs representing atoms and elastic interactions respectively. We simulate surface diffusion using an activated hopping algorithm with the hopping rate of each surface atom followed from the coordination number and the strain energy. The repeated calculations of the strain energy is the most computationally intensive part of the simulation. We handle this efficiently using a novel Green's function technique closely related to the boundary integral method.

Simulations of the morphological evolution during deposition or annealing are conducted. We observe formation of islands in both cases under a wide range of conditions. The resulting morphology resembles those of $Si_{1-x}Ge_x$ films on Si(001) substrates at low misfits.

Contents

List of Figures

Chapter 1

Introduction

"Heteroepitaxy" designates the crystal growth of a material on a substrate of a different material with the two materials being well defined in relative orientation. In most experiments, the principal axis of the film parallels that of the substrate. Since the materials of the film and the substrate are different, their lattice constants are normally different. The difference in lattice constants between the film and the substrate is called "misfit" or "mismatch", and creates an elastic strain in the film.

There are three main types of film growth: Frank-van der Merwe growth, Volmer-Weber growth and Stranski-Krastanow growth. In Frank-van der Merwe growth [Frank and van der Merwe, 1949], the film grows layer by layer. In Volmer-Weber growth [Volmer and Weber, 1926], the deposited atoms form islands on the surface. In Stranski-Krastanow growth, the film starts from layer-by-layer growth [Stranski and Krastanow, 1939] but islands are formed after a few mono-layers (figure 1.1).

The island formation in Volmer-Weber growth and Stranski-Krastanow growth can be coherent or incoherent. In coherent epitaxy, the topology of the crystal is preserved. The

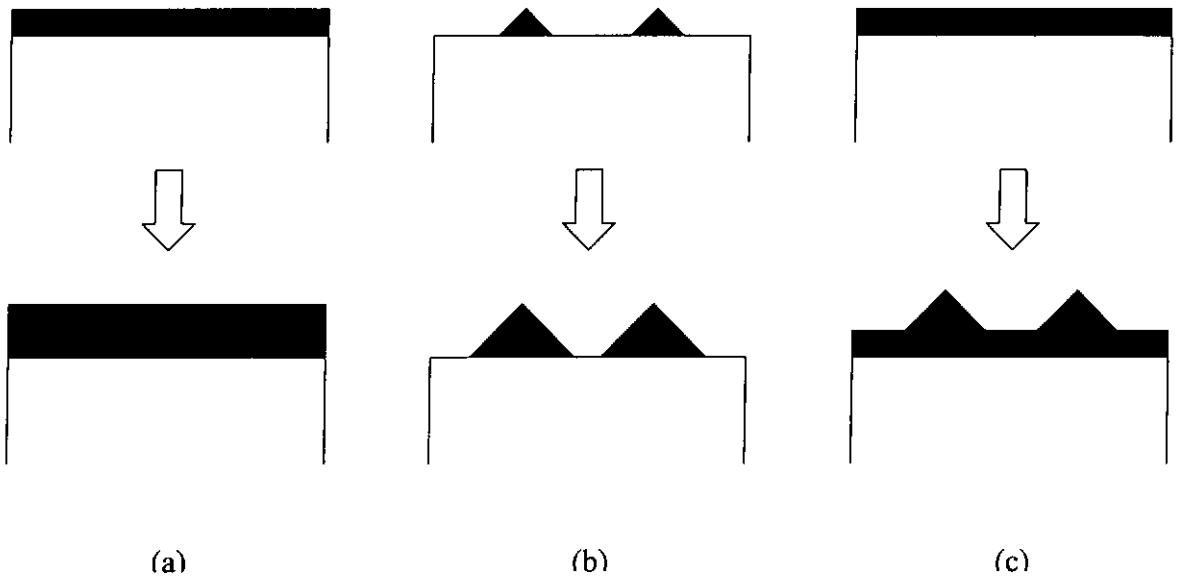

Figure 1.1: Schematic diagram of the three possible growth modes: (a) Frank-van der Merwe, (b) Volmer-Weber, and (c) Stranski-Krastanow.

formation of islands in the coherent film can partially relax the internal stress of the film caused by lattice misfit at the cost of increasing the surface energy. In incoherent epitaxy, the internal stress can also be relaxed by the formation of dislocations or dislocated relaxed islands.

Under favorable conditions, arrays of nano-size three-dimensional islands form. This may lead to a new technique for fabricating arrays of nano-size quantum dots and quantum wires, which are difficult to prepare by standard lithography. Quantum dots and quantum wires are widely expected to be useful for future micro-electronic applications, such as memory devices, single-electron transistors, and laser based on resonant wave-guiding effect.

This project focuses on the simulation of coherent Stranski-Krastanow growth of $Si_{x-1}Ge_x$ alloy on Si substrate. Growth of $Si_{x-1}Ge_x$ alloy on Si substrate with different growth parameters has been studied in many experiments [Floro *et al.*, 1999; Sutter and Lagally, 2000; Tromp *et al.*, 2000].

1.1 Experiments

Islands in heteroepitaxy can be grown by molecular beam epitaxy (MBE) and chemical vapor deposition (CVD). Molecular beam epitaxy has been used since the beginning of island formation studies. Islands formation requires slow deposition, so atoms have enough time to diffuse to favorable positions. For a long time, Stranski-Krastanow growth was believed to require dislocation, or Volmer-Weber growth will occur. However, Eaglesham and Cerullo [1990] found that Stranski-Krastanow growth of Ge on Si(100) film can be coherent. They grew the film with molecular beam epitaxy and observed it with transmission electron microscopy (TEM). The islands were dislocation-free initially until it reached the critical thickness for dislocation formation. In incoherent Stranski-Krastanow island formation, both the islands and the dislocations can relax the strain in the film. However, in coherent Stranski-Krastanow island formation, the strain can be relaxed only by the islands because dislocation is absent.

The islands in Ge/Si or $Si_{x-1}Ge_x/Si$ systems can take different shapes, such as hut, and dome shapes [Floro, 1999; Tomitori *et al.*, 1994]. When the film thickness is less than a critical thickness, the film is flat in Stranski-Krastanow growth. Ripples appear after the film grows thicker. The tilt angle of the side walls of the ripples can be 1°-3°. Upon further deposition, the tilt angle increases to 11.3°at (105) facet, and the islands change to "hut" or "pyramid" shape. A hut is bounded by four (105) facets with side wall angle of 11.3°[Mo *et al.*, 1990]. Another type of island, called "dome", can also exist. The shape of domes is more complex and includes many facets, mainly (113) facets [Kamins *et al.*, 1997; Ross *et al.*, 1999]. Domes have higher aspect ratio than huts, and relax elastic strain more effectively. Therefore, domes usually appear at greater deposited film thickness, but

domes and huts can coexist in suitable conditions.

In a film with a low Ge concentration, the shapes of the islands are similar to those in high Ge concentration, but the islands are larger. The critical thickness of the wetting layer and the size of the lateral island are found to be a function of the Ge concentration. Both quantities are roughly proportional to $1/x$ for $Si_{1-x}Ge_x/Si$ films [Sutter and Lagally, 2000; Tromp *et al.*, 2000]. A lower Ge concentration brings a lower lattice misfit, and results in larger islands and greater critical wetting layer thickness.

Experiments conducted by Floro *et al.* [1997; 1999] clearly showed the evolution of coherent Stranski-Krastanow island growth of $Si_{0.8}Ge_{0.2}$ alloy films on Si substrates. The lattice misfit is small, about 0.8%. In their experiments, the wetting layer grew two-dimensionally up to 25Å (18 mono-layers). Then rather flat islands with side walls subtending a small angle with the film surface emerged. At 65Å deposited film thickness, the islands had developed a hut shape. The huts relaxed 20% of the effective stress in the film. As growth proceeds further, mutual repulsion through elastic interactions led to increasing strains in the system. For film thickness in the range 130-210Å, the shape of the islands changed to domes and the domes relaxed 67% of the effective stress.

1.2 Theories

There are two major theories on island formation in heteroepitaxy: nucleation theory and ATG instability theory. Nucleation theory suggests that the system has to overcome an energy barrier in order to nucleate islands of a critical size [Tersoff and Tromp, 1993]. Considering the simple case that islands have identical shape at different scales, we can

find out the relation between the energies and the island size. The surface energy of the island E_{surface} is proportional to the area of the island $E_{\text{surface}} = Ah^2$, where A is a positive constant and h is the island height. The elastic energy increment E_{elastic} of the island is proportional to its volume $E_{\text{elastic}} = -Bh^3$, where B is a positive constant. It is negative because islands always release elastic energy. Then, we get the total energy $E_{\text{total}} = E_{\text{surface}} + E_{\text{elastic}} = Ah^2 - Bh^3$. From this equation, we can see that when the island is small, the surface energy dominates and the flat surface is favorable. On the other hand, when the island is large, the elastic energy released by the island dominates and the island formation is more stable.

ATG instability theory was suggested by Asaro, Tiller and Grinfeld [Asaro and Tiller, 1972; Grinfeld, 1986]. In this theory, the sinusoidal modulation on a flat surface and its strain relaxation are considered. When the amplitude of the modulation is very small, we can assume that the problem is linear. In this approach, both the relaxed elastic energy and increased surface energy are proportional to the square of the modulation amplitude. If the wavelength of the modulation is long enough, the modulation can lower the energy and the planar surface is always unstable. There is no energy barrier in the formation of islands. It is different from the nucleation theory.

The shortest wavelength λ^* for a stable modulation can be calculated from the total energy increment per unit area. The surface energy increment per unit area is found to be $E_{\text{surface}} = A\frac{h^2}{\lambda^2}$, where h and λ are the amplitude of the modulation and wavelength respectively, and A is a positive constant. The elastic energy increment per unit area is $E_{\text{elastic}} = -B\frac{h^2\varepsilon^2}{\lambda}$, where ε is the lattice misfit and B is a positive constant. Summing up the elastic and the surface energy increments per unit area, we find the total energy

increment per unit area $E_{\text{total}} = E_{\text{surface}} + E_{\text{elastic}} = (A\lambda^{-2} - B\varepsilon^2)\, h^2$. For a stable modulation, the total energy in a modulated surface is lower than that in a flat surface $A\lambda^{-2} - B\varepsilon^2 < 0$, so the wavelength should be larger than a critical value $\lambda > \lambda^* = \frac{A}{B}\varepsilon^{-2}$.

1.3 Simulations

The first kinetic Monte Carlo simulation of coherent island growth was conducted by Orr *et al.* [1992]. Their model is a two-dimensional ball-spring model. It is basically a solid-on-solid model that takes into consideration of elastic strain. Surface diffusion is modeled by hopping of surface atoms. The hopping probability of a surface atom depends on the changes in the bond energy and the elastic energy upon the removal of the surface atom. The bond energy is assumed to be proportional to the atomic coordination number. The elastic energy is calculated from equilibrating atoms in a neighborhood of size 3×3. The substrate dimensions are 75(width) $\times$ 8(height) lattice spacings. This ball-spring model is simple but can reasonably models the elastic strain. Therefore, it is used in subsequent kinetic Monte Carlo simulations.

In the simulation by Orr and his coworkers, rectangular islands were found. The island formation is more likely to be nucleation growth than ripple growth. There is no wetting layer under the islands, so the island growth is Volmer-Weber growth but not Stranski-Krastanow growth.

1.4 Scope of Investigation

As introduced in the above sections, nucleation theory, ATG instability theory and the previous atomistic simulations only partially explain island formation. In nucleation theory, the islands have to overcome an energy barrier in their formation. However, it is not suitable to explain ripple growth.

Computer simulation is another approach to understand island formation. The ball-spring model is widely used. It considers atoms and their interactions, which can better model the atoms in a film. However, previous atomistic simulations [Orr, 1992; Ratsch *et al.*, 1996; Khor and Das Sarma, 2000; Meixner *et al.*, 2001] yield nucleation growth, and ripple growth is not reported.

Another problem is the mechanism of the critical wetting layer thickness in Stranski-Krastanow growth. In the experiments [Floro *et al.*, 1999], the layer-by-layer growth can be up to 18 mono-layers. This does not appear to be due to chemical bonding between the bulk of the film and the substrate because it is a short range interaction and the effect may be too weak to extend up to 18 mono-layers. No atomistic simulation produces Stranski-Krastanow growth induced by lattice misfit.

Simulating the ripples in Stranski-Krastanow growth requires a large lattice and consideration of long range elastic interactions. Using a large lattice and calculating long range elastic interactions require a huge amount of computational power if we use only the conventional approach (section 2.4). In previous simulation studies, a small lattice and very short range of elastic interaction are used to reduce the computational time, and ripple growth does not appear. To simulate ripple growth, the main difficulty is computational speed.

In this project, we are going to simulate the strained island formation in $Si_{1-x}Ge_x$ deposited onto Si substrates. A major objective is to produce ripple growth in atomistic simulation. To realize the simulations, we have to implement a fast algorithm. Novel approaches are used to solve the problem of computational speed, which include Green's function approach (section 2.4) and super-particle approach (section 2.6). With these approaches, the computational load is reduced greatly and the calculation of long range elastic interactions on a large lattice becomes possible.

Chapter 2

Algorithms

The present research project studies heteroepitaxial growth by simulation. The model used is similar to those in previous works [Orr *et al.*, 1992; Khor *et al.*, 2000], but modifications are made to the algorithm to increase the computational speed. The faster algorithm makes it possible to simulate larger systems and reduce the computational errors.

This chapter introduces the algorithms for the simulation. To simulate an heteroepitaxial system, the film and the substrate are modeled by a network of balls and springs (the ball-spring model) as described in section 2.1. Surface diffusion is also needed because it is the major mechanism to develop the surface morphology to form islands. Surface diffusion is simulated by activated hopping of surface atoms. The hopping algorithm will be introduced in section 2.2.

For the hopping of surface atoms, we need to know their activation energy. However, the calculation of the elastic part of the energy is very time consuming. A Green's function approach (section 2.4) and a super-particle approach (section 2.6) are used to increase the speed of the elastic energy calculation. An energy estimation table (section 2.7) is

compiled to reduce the frequency of the elastic energy calculation, so as to increase the simulation speed. Using the algorithms in this chapter, we can do fast simulations to study the island formation process.

2.1 Ball-spring model

A film on a substrate is studied using a two dimensional model. Atoms and bonds are represented by balls and springs. Horizontal and vertical springs connect nearest neighboring atoms, and diagonal springs connect next nearest neighbors. Altogether, there are eight bonds for each bulk atom. Figure 2.1 shows a small lattice of a flat film and the eight bonds connected to a bulk atom.

The springs define the elastic properties of the material. Different elastic modulus is modeled by different spring constants. The lattice misfit is modeled by a difference between the natural lengths of the springs in the film and those in the substrate. Shorter springs in the substrate result in a compression strain in the film.

As the substrate is much thicker than the film, it is assumed that there is no strain at locations in the substrate far from the interface. Therefore, the atoms at the bottom row in our model are fixed, and the separations between the atoms at the bottom row are equal to the lattice constant of the substrate.

The atomic positions in a perfectly flat film define a convenient reference lattice and the lattices representing the substrate and the film are arranged in square and rectangular lattices respectively. The aspect ratio of the film lattice can be easily found by solving the equilibrium positions of the film atoms. The dotted lines in figure 2.1 indicate the

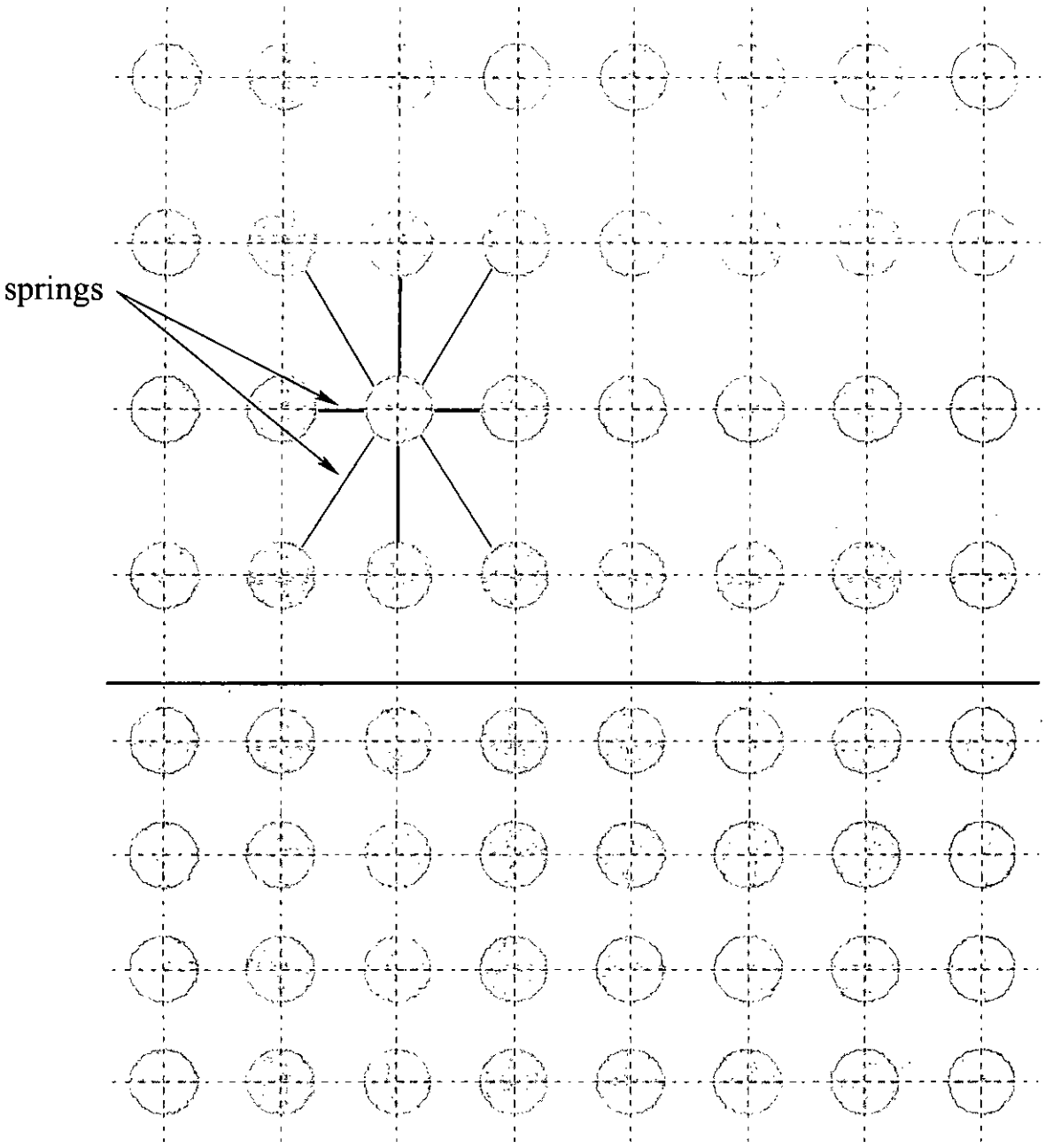

Figure 2.1: Small scale model of a flat film. Atoms in a flat film define the reference lattice. The solid circles and the grid of dotted lines represent the atoms and the reference lattice respectively. The horizontal solid line indicates the interface between the film and the substrate. Every atom is connected directly to its nearest and next nearest neighbors. Eight bonds of a bulk atom is shown.

reference lattice. All the atoms in the figure are located on the lattice points because the surface is flat.

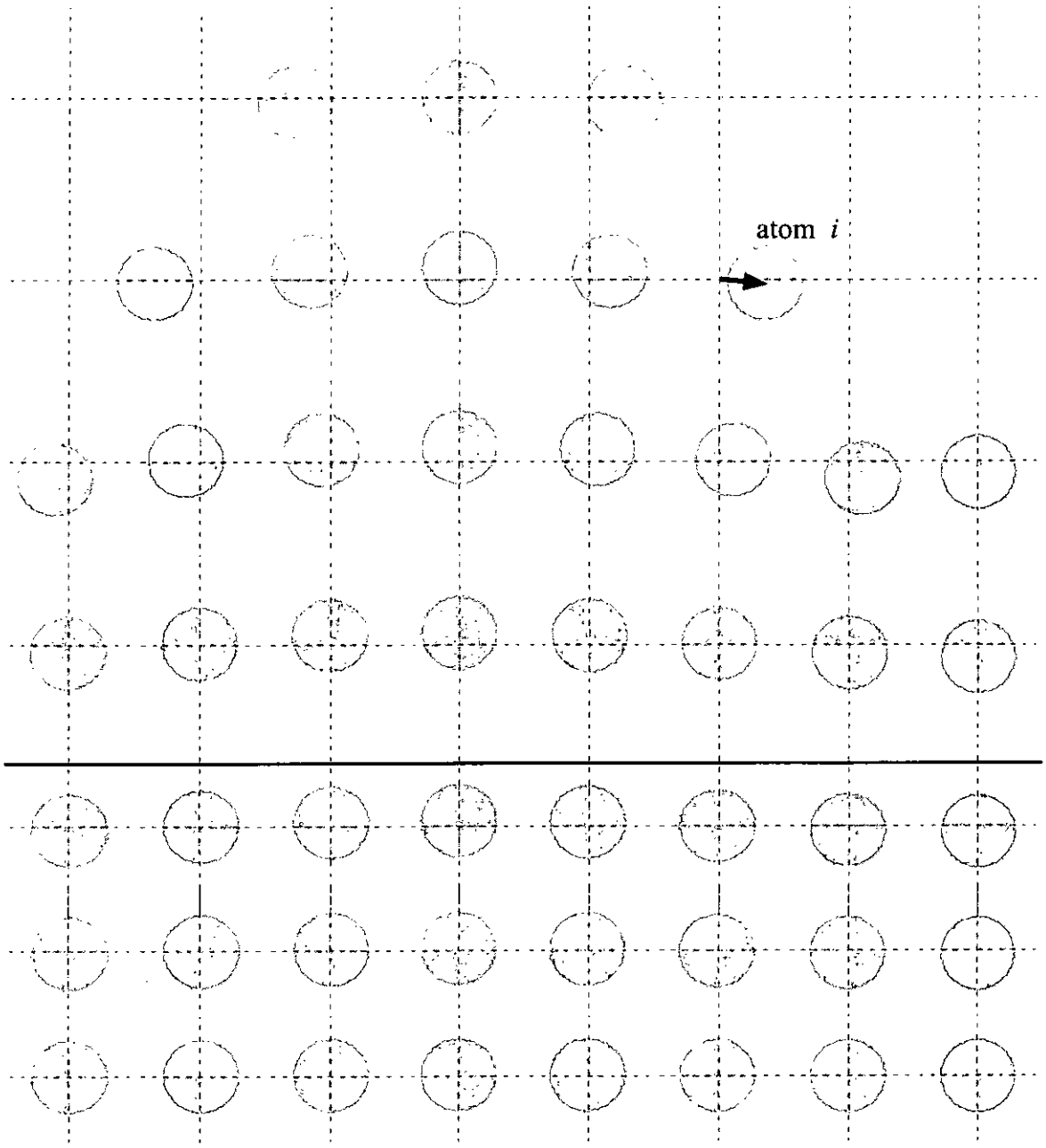

Figure 2.2: In a rough surface, the displacement vector $\mathbf{u}_i$ of an atom i from its regular lattice position is shown by the arrow.

In the case of a rough surface, the atoms no longer sit on the reference lattice. There is a displacement $\mathbf{u}_i$ for each atom i referred from its lattice point. The reference lattice and the displacements provide enough information on the positions of the atoms, so the

elastic energy stored in the springs as well as the spring force can be expressed in terms of $\mathbf{u}_i$. This notation helps reduce the complexity of the equations. Figure 2.2 shows a rough surface. Displacement $\mathbf{u}_i$ of atom i is indicated by an arrow, which points to the atom from its lattice point.

For a pair of neighboring atoms, atom i and atom j, elastic force $\mathbf{f}_{ij}$ applied on atom i from atom j is given by Hook's law:

$$\mathbf{f}_{ij} = -k_{ij}\left(|\mathbf{r}_{ij}| - l_{ij}^0\right)\hat{\mathbf{r}}_{ij} \tag{2.1}$$

where k_{ij} is the spring constant equivalent to either k_N or k_{NN} for nearest or next nearest neighbors respectively. l_{ij}^0 is the natural length of the spring. Vector $\mathbf{r}_{ij}$ points from atom j to atom i and is given by

$$\mathbf{r}_{ij} = \mathbf{u}_i - \mathbf{u}_j + \mathbf{l}_{ij} \tag{2.2}$$

where $\mathbf{l}_{ij}$ is the vector pointing from the lattice point j to i. The spring force is given by

$$\begin{aligned}\mathbf{f}_{ij} &= -k_{ij}\hat{\mathbf{l}}_{ij}\hat{\mathbf{l}}_{ij}^t\left(\mathbf{u}_i - \mathbf{u}_j\right) + k_{ij}\hat{\mathbf{l}}_{ij}\left(l_{ij}^0 - |\mathbf{l}_{ij}|\right) \\ &\quad + \frac{k_{ij}}{|\mathbf{l}_{ij}|}\hat{\mathbf{e}}_{ij}\hat{\mathbf{e}}_{ij}^t\left(\mathbf{u}_i - \mathbf{u}_j\right)\left(l_{ij}^0 - |\mathbf{l}_{ij}|\right) + \mathcal{O}\left(|\mathbf{u}_i - \mathbf{u}_j|^2\right)\end{aligned} \tag{2.3}$$

where $\hat{\mathbf{l}}_{ij}$ is the unit vector of $\mathbf{l}_{ij}$, and $\hat{\mathbf{e}}_{ij}$ is a unit vector perpendicular to $\hat{\mathbf{l}}_{ij}$. Assuming that both $|\mathbf{u}_i - \mathbf{u}_j|$ and $\left(l_{ij}^0 - |\mathbf{l}_{ij}|\right)$ are small, we neglect the term $\frac{k_{ij}}{|\mathbf{l}_{ij}|}\hat{\mathbf{e}}_{ij}\hat{\mathbf{e}}_{ij}^t\left(\mathbf{u}_i - \mathbf{u}_j\right)\left(l_{ij}^0 - |\mathbf{l}_{ij}|\right)$ and the higher order terms $\mathcal{O}\left(|\mathbf{u}_i - \mathbf{u}_j|^2\right)$. Then, we have

$$\mathbf{f}_{ij} = -\mathbf{K}_{ij}(\mathbf{u}_i - \mathbf{u}_j) + \mathbf{b}_{ij} \tag{2.4}$$

where $\mathbf{K}_{ij}$ is a 2×2 matrix analogous to the elastic modulus tensor and given by

$$\mathbf{K}_{ij} = k_{ij}\hat{\mathbf{l}}_{ij}\hat{\mathbf{l}}_{ij}^{t} \tag{2.5}$$

and $\mathbf{b}_{ij}$ is a column vector defined as

$$\mathbf{b}_{ij} = (l_{ij}^{0} - |\mathbf{l}_{ij}|)\mathbf{K}_{ij}\hat{\mathbf{l}}_{ij} \tag{2.6}$$

Total energy E of the system consisting of bond energy E_b and elastic energy E_s, i.e. $E = E_b + E_s$. The bond energy E_b is defined as

$$E_b = n_N\gamma_N + n_{NN}\gamma_{NN} \tag{2.7}$$

where γ_N and γ_{NN} are the bond energies for nearest and next nearest neighbors respectively while n_N and n_{NN} are the respective numbers of bonds in the system. The elastic energy E_s of a system is defined as the sum of the elastic energy stored in all the springs when the whole network is at mechanical equilibrium. In this notation, bond energy E_b is negative so that it is more favorable to forming more bonds, but elastic energy E_s is always positive.

Simplifications are applied on elastic energy calculation. The elastic couplings of adatoms with the rest of the system are weak and are completely neglected for better computational efficiency. The height of surface steps is limited to no more than two atoms tall. This limitation is realized by defining the energy of a system to be positive infinity if the height of any surface step is greater than two atoms. These are the major

modifications from the ball-spring model of Orr *et al.* [1992].

2.2 Atomic Hopping Rates

Surface diffusion is simulated by hoppings of the topmost atoms in the film. Every topmost atom can hop to a random topmost site s columns away where $s = \pm 1, \pm 2, \ldots,$ or $\pm s_{\max}$ with equal probability. Previous simulations [Orr *et al.*, 1992; Barabási, 1997; Khor and Das Sarma, 2000] allowed only nearest neighbor hopping (i.e. $s_{\max} = 1$). Solid-on-solid (SOS) condition is assumed.

The hopping rate Γ_m of a topmost atom m follows an Arrhenius form:

$$\Gamma_m = R \exp\left(-\frac{\Delta E_m + E_0}{k_B T}\right) \tag{2.8}$$

where k_B and T are the Boltzmann constant and the temperature respectively, and ΔE_m is the change in the energy of the system upon removal of the atom m. We set the rate constant $R = 2D_0/(a_s^2\sigma^2)$, where D_0 and a_s are the diffusion coefficient and the lattice constant respectively. The variance σ^2 of the hopping distance can be calculated with the equation $\sigma^2 = \frac{1}{6}(s_{\max}+1)(2s_{\max}+1)$. We define $E_0 = E_a - (\gamma_N + 2\gamma_{NN})$, where E_a is the adatom hopping energy barrier on a flat surface. The total energy change ΔE_m can also be divided into bond energy change $\Delta E_{b,m}$ and elastic energy change $\Delta E_{s,m}$, such that $\Delta E_m = \Delta E_{b,m} + \Delta E_{s,m}$. Physically, a weakly bonded atom for which $\Delta E_{b,m}$ is less positive, or highly stressed for which $\Delta E_{s,m}$ is more negative, is more likely to hop. Our model follows detailed balance.

In the simulation of film growth, the knowledge of the elastic energy change $\Delta E_{s,m}$

is in principle required during each atomic hop attempt as implied by equation (2.8). The repeated calculation of $\Delta E_{s,m}$ is computationally very intensive and is the reason why kinetic Monte Carlo simulation of strained layers is technically a much more challenging problem than its strain-free counterpart. To conduct large scale simulations with good accuracy, the critical task is not only to implement efficient relaxation algorithm for calculation of $\Delta E_{s,m}$ but, equally important, also to devise a hopping algorithm which minimize the number of such calculations.

2.3 Sampling of Hopping Events

We apply an event acceptance-rejection scheme to reduce the number of elastic energy calculations required in our hopping algorithm. The lower and upper bounds ΔE_m^{min} and ΔE_m^{max} respectively of ΔE_m for all surface atoms are estimated. The algorithm of energy estimation will be described in section 2.7. Assume that ΔE_m^{min} is known, we consider a hop attempt by the surface atom at m-th column with a rate

$$\Gamma_m^a = R \exp\left(-\frac{\Delta E_m^{min} + E_0}{k_B T}\right) \tag{2.9}$$

A hop attempt at an arbitrary column occurs at rate $\Gamma^a = \sum_m \Gamma_m^a$. On average, such an event happens after the average time interval $\Delta t = 1/\Gamma^a$ has elapsed. The hop attempt should occur at the m-th column with the probability Γ_m^a/Γ^a. We sample m from this distribution efficiently with the help of a binary tree data structure. An attempt sampled

is only successful with the probability

$$p_m = \exp\left(-\frac{\Delta E_m - \Delta E_m^{min}}{k_B T}\right) \tag{2.10}$$

because the hopping rate $\Gamma_m = \Gamma_m^a p_m$ should hold.

The data structure of a binary tree is used to sample the atom m to hop. Figure 2.3 is an example of a small binary tree. The circles represent nodes and every node stores a numerical value. A node can have at most two child nodes, the left child and the right child. Similar to usual binary trees, the nodes at the bottom are called "leaves" and the node at the top is called "root".

Leaves store the value of Γ_m^a and every parent contains the sum of values of its children, so the root node will contain the value Γ^a. Since the number of leaves is known to be equal to the lattice width, the size of the tree is constant.

To choose a surface atom to hop, a binary search is used. We starts the search from the root node. A uniformly distributed random number $\zeta \in [0, \Gamma^a)$ is generated. Then, ζ is compared to the value of the left child. If ζ is greater than the value of the left child, we move to the right child and reduces ζ by the value of the left child; otherwise, we move to the left child and ζ remains unchanged. Comparing repeatedly ζ to the children and moving down the tree, we will reach a leaf at the end. The final leaf is the result, which represents the surface atom that will attempt to hop in acceptance-rejection process.

After a surface atom is chosen, an acceptance-rejection process will start to test whether the atom can hop or not. The probability of accepting a hop is p_m. Despite its appearance in p_m, ΔE_m still may not need to be calculated if we apply the known lower bound p_m^{min}

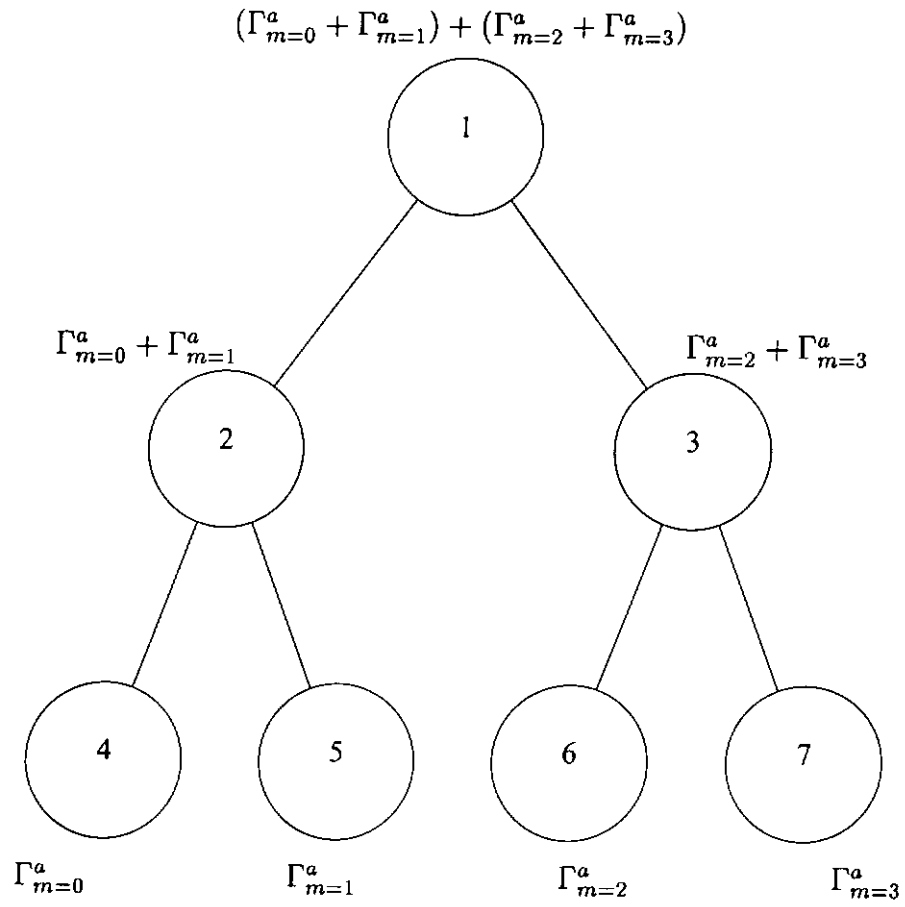

Figure 2.3: Binary tree for a small 4-column-wide lattice. The circles represent nodes and the numbers in circles are the indexes of the nodes.

of p_m defined as

$$p_m^{min} = \exp\left(-\frac{\Delta E_m^{max} - \Delta E_m^{min}}{k_B T}\right) \tag{2.11}$$

where ΔE_m^{max} and ΔE_m^{min} are respectively the estimation of upper and lower boundary of the change in elastic energy.

We first sample a uniform random number $\xi \in [0, 1)$. If $\xi \leq p_m^{min}$, the hopping attempt will be accepted right away. Otherwise, we come to the point that ΔE_m will actually be computed to give p_m. The attempt is then accepted if and only if the same ξ, which is already found to satisfy $\xi \geq p_m^{min}$, follows $\xi \leq p_m$. With this scheme, there is a probability p_m^{min} that it is not necessary to calculate the value of ΔE_m.

2.4 Green's Function Approach

Conventionally, one consider the mechanical equilibrium for atom i as the net force by all springs vanishes, i.e.

$$\sum_i \mathbf{f}_{ij} = 0 \tag{2.12}$$

where the sum is over all directly connected neighbors j. Let n be the total number of atoms in both the film and the substrate. Application of equation (2.12) leads to a set of $2n$ linear scalar equations for which the vector displacement $\mathbf{u}_i$ for all atoms can be solved. The elastic energies in all springs are then summed up to give the elastic energy of the system. However, solving large number of equations is a CPU intensive process. It is necessary to improve the efficiency of the elastic energy calculations.

We now introduce a fast algorithm for computing elastic energy which involves ex-

plicit consideration of only surface atoms. This reduces the complexity of the problem effectively by one dimension and provide significant speed up. This is a lattice analog of boundary integral methods and the derivation is nevertheless simpler and allows transparent physical interpretations. The idea is as follows. Atoms in the bulk are intrinsically coupled into the problem because they are important in mediating elastic interactions between surface atoms. Now, we eliminate their explicit reference by representing these indirect long-range interactions using appropriate lattice Green's functions.

Specifically, consider an extended network of balls and springs with a flat upper boundary. It differs from the growing film by having extra atoms with identical elastic properties to those in the film. We call these imaginary atoms (figure 2.4). The springs connecting the imaginary and the real atoms are unphysical. However, we can fix this by applying external forces $\mathbf{f}_k^e$ acting on each real surface atom k so that the net unphysical forces vanishes, i.e.

$$\mathbf{f}_k^e + \sum_{k'} \mathbf{f}_{kk'} = 0 \tag{2.13}$$

The sum is over all imaginary neighbors k' directly connected to k. Applying equation (2.4), we get

$$\mathbf{f}_k^e = \sum_{k'} \left[\mathbf{K}_{kk'} \ (\mathbf{u}_k - \mathbf{u}_{k'}) - \mathbf{b}_{kk'}\right] \tag{2.14}$$

The dependence on $\mathbf{u}_{k'}$ is undesirable. We hence apply to each imaginary surface atom k' a further external force $\mathbf{f}_{k'}^e$ satisfying

$$\mathbf{f}_{k'}^e + \sum_{k} \mathbf{f}_{kk'} = \sum_{k} \mathbf{b}_{k'k} \tag{2.15}$$

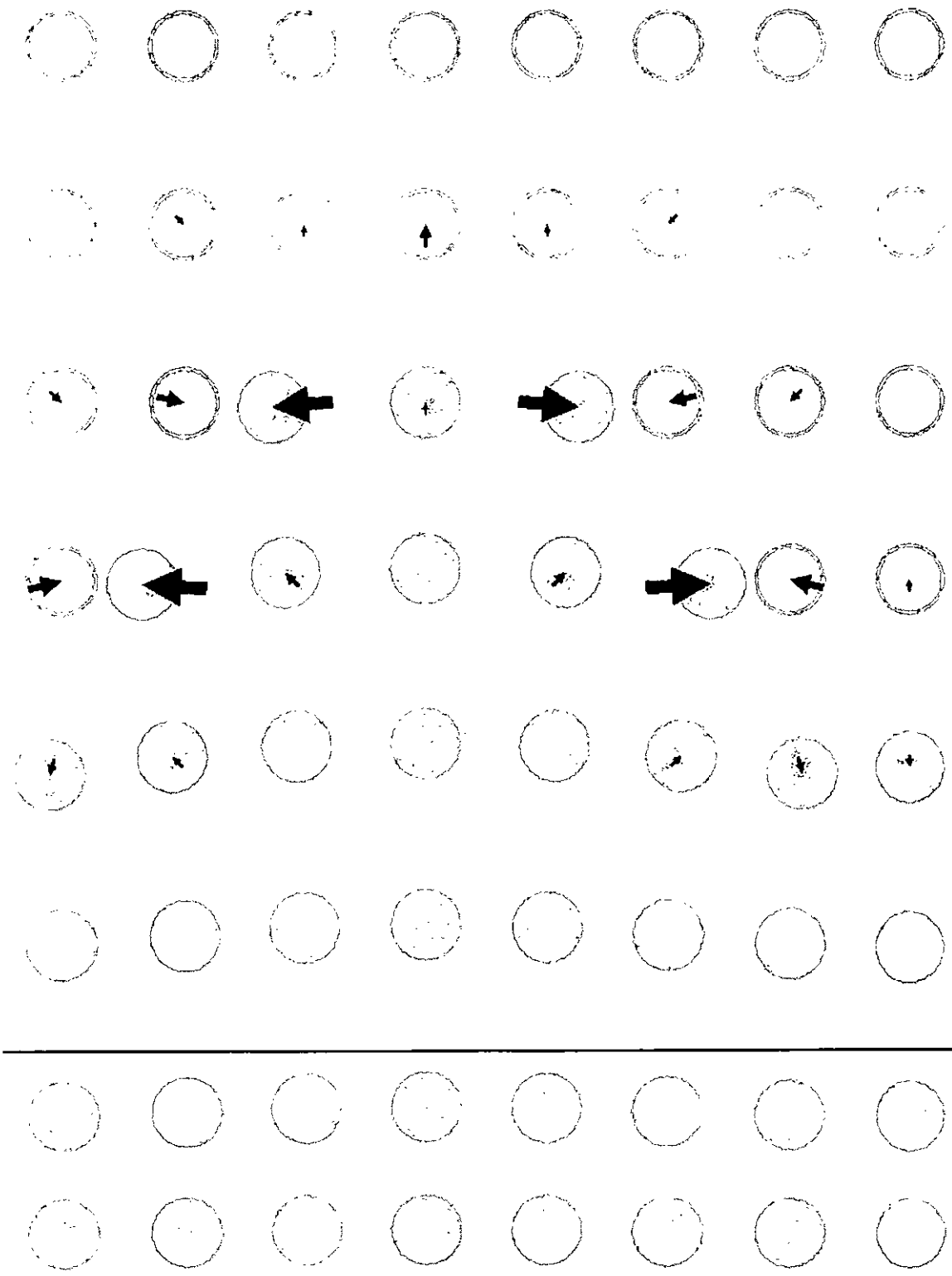

Figure 2.4: An extended model of a strained film with imaginary film atoms added on top. The arrows show the external forces $\mathbf{f}_k^e$ and $\mathbf{f}_{k'}^e$ acting respectively on real (solid circle) and imaginary (open circle) surface atoms so as to cancel all elastic effects of the imaginary region on the real one.

where both sums are over all real neighbors k of k'. It states that the total force exerted on k' by all neighboring real atoms, after supplemented by $\mathbf{f}^e_{k'}$, is as if the real surface atoms were at their reference lattice position. Therefore, the obvious solution for all imaginary atoms is

$$\mathbf{u}_{k'} = 0 \tag{2.16}$$

The external forces can now be expressed as

$$\mathbf{f}^e_k = \sum_{k'} (\mathbf{K}_{kk'} - \mathbf{b}_{kk'}) \tag{2.17}$$

$$\mathbf{f}^e_{k'} = -\sum_{k} \mathbf{K}_{kk'}\mathbf{u}_k \tag{2.18}$$

where we have also used the equations (2.5) and (2.6), $\mathbf{K}_{kk'} = \mathbf{K}_{k'k}$ and $\mathbf{b}_{kk'} = \mathbf{b}_{k'k}$. In summary, after applying $\mathbf{f}^e_k$ and $\mathbf{f}^e_{k'}$ to respectively real and imaginary surface atoms, the real atoms are free from the effects of any unphysical forces and they sit at their proper equilibrium positions, while all imaginary atoms are at their reference lattice positions.

To close the equations, we first have to define a lattice Green's function for the extended network. When an arbitrary force $\mathbf{f}_j$ is applied to any atom j, Green's function $\mathbf{G}_{ij}$, which is a 2×2 matrix function of i and j, expresses the displacement of atom i as

$$\mathbf{u}_i = \mathbf{G}_{ij}\mathbf{f}_j \tag{2.19}$$

An important point is that $\mathbf{G}_{ij}$ is a Green's function for the extended network, instead of the original one representing only real atoms, and is hence independent of the instantaneous film configuration. Before commencing a simulation, it is first numerically

computed using conventional equations for mechanical equilibrium similar to equation (2.12), but with applied force $\mathbf{f}_j$ accounted for. The boundary condition is same as the original network except that the top row of imaginary atoms are also fixed. Therefore, periodic boundary condition is applied on the left and right margin, and the atoms at the top and bottom rows are fixed. There is a translation symmetry in the horizontal direction of $\mathbf{G}_{ij}$. It helps reducing the number of computations and the storage requirement greatly. However, it lacks a similar symmetry in the vertical direction.

Applying the Green's function, the displacement of any atom is given by

$$\mathbf{u}_i = \sum_j \mathbf{G}_{ij}\mathbf{f}_j^e + \sum_{j'} \mathbf{G}_{ij'}\mathbf{f}_{j'}^e \tag{2.20}$$

Substituting this equation into the expressions for the external forces in equations (2.15) and (2.17), we have

$$\mathbf{u}_i = \sum_j \sum_{j'} \mathbf{G}_{ij}\ (\mathbf{K}_{jj'}\mathbf{u}_j - \mathbf{b}_{jj'}) - \sum_{j'} \sum_j \mathbf{G}_{ij'}\mathbf{K}_{jj'}\mathbf{u}_j \tag{2.21}$$

It is then simplified to

$$\mathbf{u}_i = \sum_j \sum_{j'} \left[(\mathbf{G}_{ij} - \mathbf{G}_{ij'})\ \mathbf{K}_{jj'}\mathbf{u}_j - \mathbf{G}_{ij}\mathbf{b}_{jj'}\right] \tag{2.22}$$

The double summation is over all real and imaginary surface atoms j and j' respectively which are directly connected neighbors. For n_s real surface atoms, there are n_s linear equations of equation (2.22) for all $\mathbf{u}_i$. Solving the system of equations, we can get displacements $\mathbf{u}_i$ for all surface atoms, hence the elastic energy of the system can be

found.

For example, a simulation with substrate dimension 1024 × 1024. The number of linear equations in conventional approach using equation (2.12) is over 2 million, but the number of equations in Green's function approach using equation (2.22) is roughly only 2 thousand. It saves a lot of CPU time and memory usage.

2.5 Elastic Energy Calculation

The elastic energy E_s of a system is defined by the sum of the elastic energy stored in all springs, and is given by the equation

$$E_s = \sum_{ij} \frac{k_{ij}}{2} \left[(\mathbf{u}_i - \mathbf{u}_j)\, \hat{\mathbf{n}}_{ij} + l^0_{ij} - l_{ij} \right]^2 \tag{2.23}$$

The double summation is over all directly bonded neighboring atoms i and j. As in the previous sections, the vector $\mathbf{u}_i$ is the displacement of atom i from its lattice point; k_{ij} is the spring constant; $\hat{\mathbf{n}}_{ij}$ is the normal vector pointing from lattice point of atom i to that of atom j; l^0_{ij} is the natural length of the springs, and l_{ij} is the atomic separation in the reference lattice.

Calculating the total elastic energy directly using equation (2.23) is not efficient because it requires to know the displacements of all the atoms. Therefore, a fast algorithm is used after the the displacement of surface atoms is calculated using the Green's function approach. It needs only the displacements of the surface atoms, but not those of the bulk atoms.

We consider the original network which consists of only film and substrate atoms, but

imaginary atoms and unphysical springs do not exist anymore. Then, virtual forces $\mathbf{f}_k^v$ applied to every surface atom k are gradually turned on pushing atoms adiabatically back to their reference lattice positions. It is again easy to see that $\mathbf{f}_k^v$ is given by

$$\mathbf{f}_k^v = \sum_{k'} \mathbf{b}_{kk'} \tag{2.24}$$

which sums over neighboring imaginary atomic positions k' even though imaginary atoms are no longer present. The virtual work done is

$$W = \frac{1}{2} \sum {}_k \mathbf{f}_k^v \cdot (-\mathbf{u}_k) = -\frac{1}{2} \sum_{kk'} \mathbf{b}_{kk'} \cdot \mathbf{u}_k \tag{2.25}$$

Let E_s^{ref} be the strain energy when all the atoms are at their reference lattice positions, which can be calculated straightforwardly from simple bond counting. There are eight bonds for each bulk atom, so we actually count the number of bulk atoms and the number of bonds for surface atoms only. Elastic energy E_s is then computed from

$$E_s = E_s^{ref} - W \tag{2.26}$$

Our application of equations (2.22) and (2.26) to calculate respectively the displacement vectors $\mathbf{u}_i$ and hence the strain energy E_s involves surface atoms only. Calculation of the displacements of the bulk atoms are unnecessary but can be carried out also using equation (2.22) with known values of $\mathbf{u}_k$ on the right hand side. We do this only occasionally for self-consistency check or graphic display.

2.6 Super-Particle

A super-particle approach is used to improve the performance of the calculation of $\Delta E_{s,m}$, where $\Delta E_{s,m}$ is the elastic energy change upon the removal of the atom m. The Green's function approach described in section 2.4 and the elastic energy calculation algorithm described in section 2.5 are exact for our lattice model. In contrast, a super-particle approximation will now be taken.

The local strain changes little when it is far away from atom m. In the calculation of elastic energy change $\Delta E_{s,m}$, the surface atoms are divided into many groups and each group is called a "super-particle". We assume that all the atoms in a super-particle have the same displacement $\mathbf{u}_i$, so the number of unknowns is reduced. With fewer unknowns, the calculation speed is increased.

The super-particle size depends on its distance r from atom m. The super-particles are larger if farther away. Within $r < r_0$ columns away from atom m, the atoms are not grouped, where r_0 is a constant to control the super-particle sizes. The ungrouped atoms are treated as a super-particle containing only a single atom. For atoms farther away, where $r \geq r_0$, the super-particle size is assigned to $2r/r_0 - 1$ columns. Here, the term "surface atom" means an atom having fewer than eight bonds.

For example, the grouping of surface atoms with $r_0 = 3$ is shown in figure 2.5. The surface atoms at the nearest 7 columns, including the column of atom m, are not grouped. Each surface atom close to atom m is also treated as a super-particle that contains only one single atom. Then, at the forth columns to the left and to the right, the super-particles are 3 columns in width. Super-particles with sizes 5 and 9 are followed.

In the super-particle approach, we neglect fluctuations within a set by assuming iden-

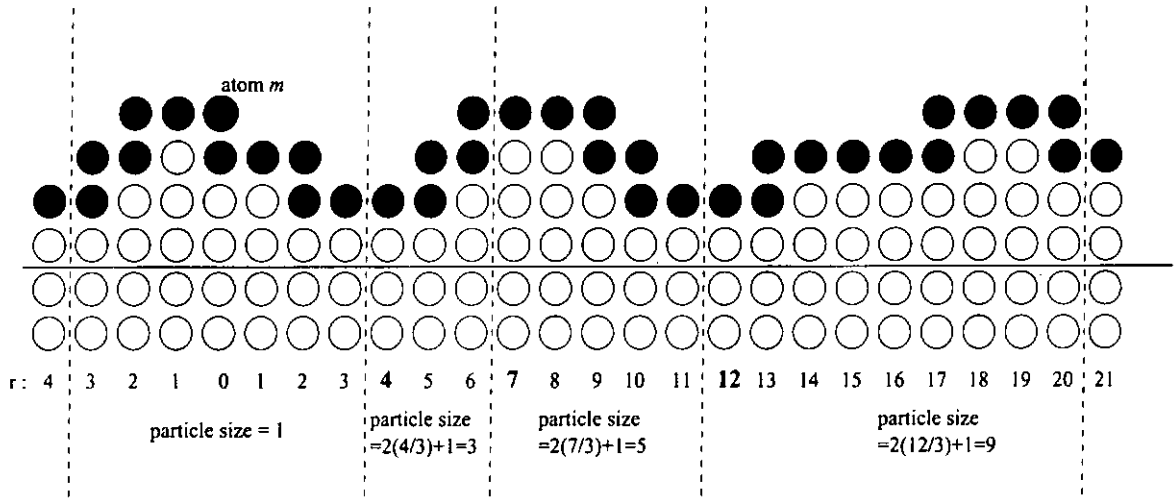

Figure 2.5: An example of grouping surface atoms to super-particles with $r_0 = 3$ while $\Delta E_{s,m}$ calculation. The numbers under the columns are the distance from the atom m, which attempts to hop. Surface atoms are shaded in gray. Dotted lines divide the surface atoms into groups.

tical displacement $\mathbf{u}_i \equiv \mathbf{u}_I$ for each member $i \in \Omega_I$, where Ω_I denotes the set of the atoms constituting super-particle I. Equation (2.22) is then modified as follows:

$$\begin{aligned} \mathbf{u}_i &= \sum_j \sum_{j'} [(\mathbf{G}_{ij} - \mathbf{G}_{ij'})\, \mathbf{K}_{jj'} \mathbf{u}_j - \mathbf{G}_{ij} \mathbf{b}_{jj'}] \\ &= \sum_J \sum_{j \in \Omega_J} \sum_{j'} [(\mathbf{G}_{ij} - \mathbf{G}_{ij'})\, \mathbf{K}_{jj'} \mathbf{u}_j - \mathbf{G}_{ij} \mathbf{b}_{jj'}] \\ \Rightarrow \quad \mathbf{u}_I &\approx \sum_J \left\{ \left[\sum_{j \in \Omega_J} \sum_{j'} (\mathbf{G}_{Ij} - \mathbf{G}_{Ij'})\, \mathbf{K}_{jj'} \right] \mathbf{u}_J - \sum_{j \in \Omega_J} \sum_{j'} \mathbf{G}_{Ij} \mathbf{b}_{jj'} \right\} \end{aligned} \tag{2.27}$$

where $G_{Ij} = G_{ij}$ with the lattice point i at the centroid of the set Ω_I.

Solving equation (2.27) with bi-conjugate gradient method [Press, 1992], we can get the displacements of the surface atoms. Hence, elastic energy E_s of the system is calculated with the method described in section 2.5. Elastic energies E_s for the surface with and without atom m are calculated, and the difference, defined as the elastic energy change $\Delta E_{s,m}$, is applied to equation (2.8).

Using this approach, the number of equations can be reduced and the time for it takes

to solve the equations can also be reduced. For example, without the super-particle approach for a lattice width 1000, there are about 1000 surface atoms and about 2000 equations. With super-particle, there are about 30 super-particle and about 60 equations only. Therefore, the super-particle approach can improve the performance by about 1000 times.

2.7 Elastic Energy Estimation Table

We estimate the lower and upper bounds ΔE_m^{min} and ΔE_m^{max} respectively of ΔE_m with the local surface configuration near the atom m. A local configuration is assigned 9 columns in width, i.e. 8 steps. There are 5 choices for each step, either 0, ± 1, or ± 2 (figure 2.6). Totally, there are $5^8 = 390625$ configurations. Wider local region with larger number of configurations is supposed to help better estimation of ΔE_m because it gives more information about the surface. However, the number of configurations is limited by the computer memory and the calculation speed, so this width is chosen with considering both the performance and limitation of resource.

Before running simulations, we compute ΔE_m for all local configurations. The environment outside the local region is set to a flat surface of 8 layers higher than the central column of the configuration (figure 2.6). Then, we define Ψ_C as the elastic energy $\Delta E_{s,m}$ of a local configuration C.

For a local configuration, $\Delta E_{s,m}$ is proportional to the stress applied, which is caused by the misfit and the deformation of the outer surface. In the simulation, we can take an

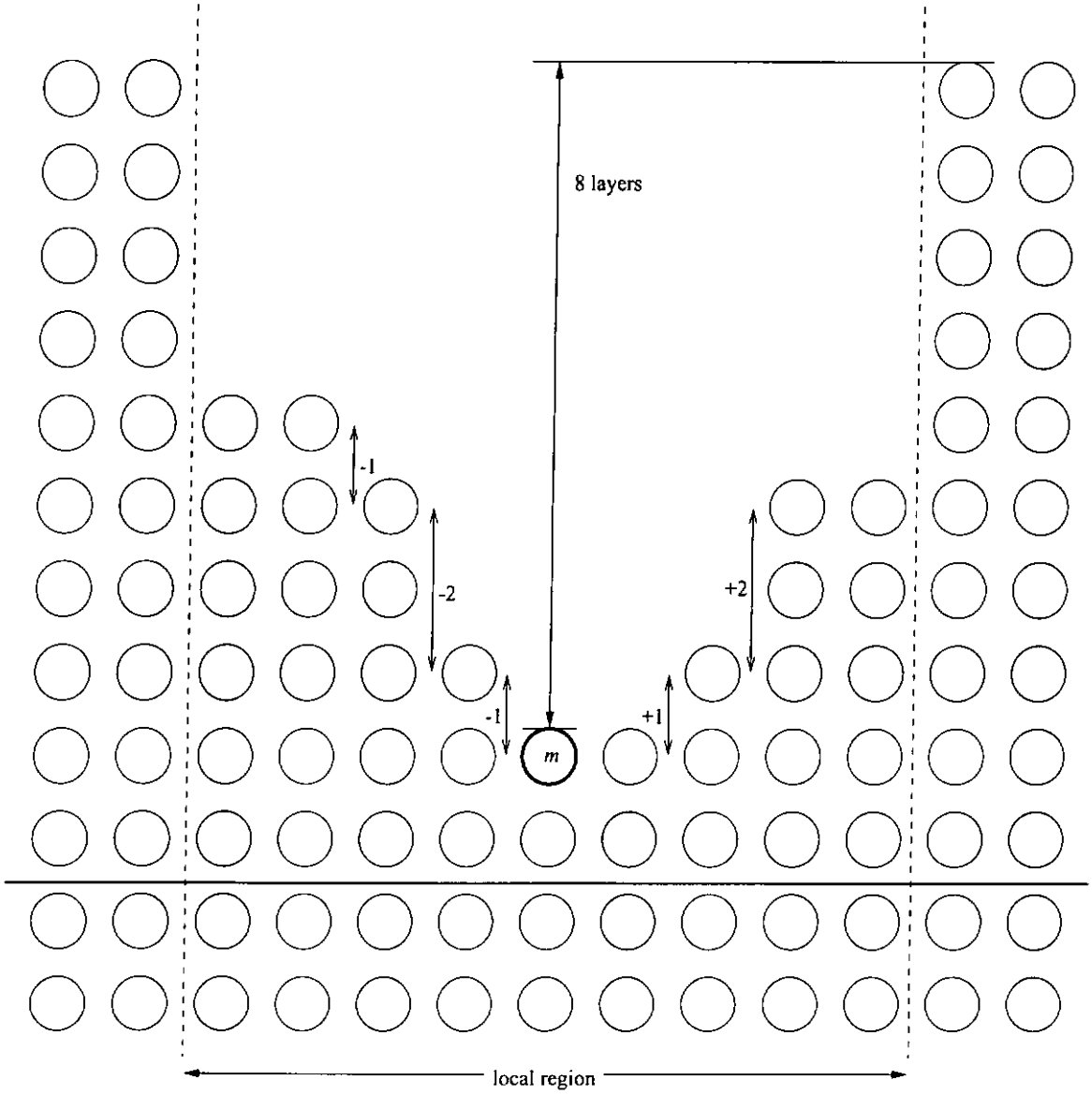

Figure 2.6: A segment of the surface for computing local configuration table. The local region is indicated by two vertical dotted lines. In the local region surrounding atom m, the step size can be either -2, -1, 0, $+1$, or $+2$. The width of local region is 9 lattice spacing. When calculating the local configuration table, the environment is a flat surface 8 layers higher than atom m.

approximation that the square of the stress is

$$\psi^2 = \frac{\Delta E_{s,m}}{\Psi_C} \tag{2.28}$$

During a simulation, we assume the change in ψ^2 is slow because the change in surface morphology is slow. Once ψ^2 has been found, it is used to estimate the bounds of ΔE_m for the next few hopping attempts until ΔE_m is calculated and ψ^2 is updated with equation (2.28).

We estimate the bounds of ΔE_m with the equations

$$\Delta E_m^{min} = \Delta E_{b,m} + \left(\psi^2 + c_1\right)\Psi_C - c_2 \tag{2.29}$$

$$\Delta E_m^{max} = \Delta E_{b,m} + \left(\psi^2 - c_1\right)\Psi_C + c_2 \tag{2.30}$$

where c_1 and c_2 are constants. We choose the value of c_1 and c_2, so that ΔE_m falls in between ΔE_m^{max} and ΔE_m^{min} with a 99% chance. When the difference between ΔE_m^{max} and ΔE_m^{min} is small, fewer calculations of ΔE_m are required because p_m^{min} in equation (2.11) is smaller. When the bounds are closer to ΔE_m, the acceptance rate in equation (2.10) is higher.

Chapter 3

Software Implementation

In this chapter, more computational details are described, such as the main program structure, the use of distributed computing and graphic display. With these modules, data analysis, process controlling and program debugging become easier and more effective.

3.1 Main Simulation Programs

The software package includes the hopping procedures, an energy calculation module, a file operation module, a graphic display and user interfacing module, a program for the calculation of the Green's function, a program for the calculation of the energy estimation table, program testing and efficiency analysis modules, programs for data processing, and programs for jobs controlling in the distributed computing environment.

Figure 3.1 shows the structure of the software package. The energy estimation table is an array containing Ψ_C (section 2.7) for the estimation of the upper and the lower bounds of the energy changes. The Green's function is the values of $\mathbf{G}_{ij}$ introduced in section

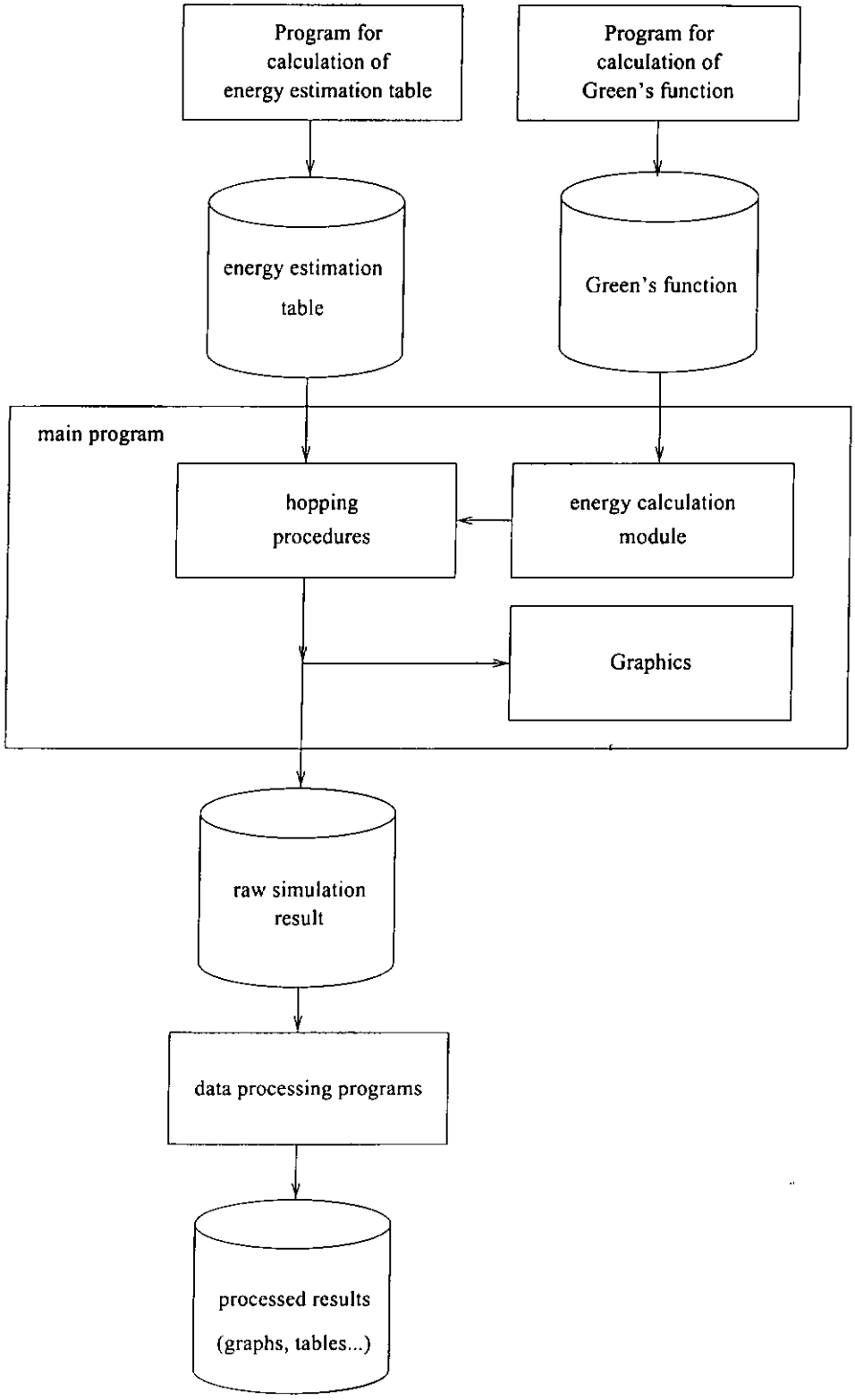

Figure 3.1: Structure of the software packages. The rectangles represent the programs and modules. The cylinders and the arrows represent the data stored in hard disk and the data flows respectively.

2.4. Both the energy estimation table and the Green's function are stored in the hard disk, and are loaded into memory at the beginning of a simulation.

The main program simulates the formation of islands. There are four main modules in the main program. They are the hopping procedures, energies calculation module, graphic module and file operation modules. The hopping procedures process the hoppings of the surface atoms using the hopping algorithm in section 2.2. The energies calculation module is highly optimized because the elastic energy calculation is the bottleneck of the performance although the Green's function approach and super-particle approach are used. The graphic module can display the information of the film during or after the simulation.

The programs are mainly written in C++, Perl and Unix shell script language. C++ is used in the main program for the calculation of the Green's function and the elastic estimation table. Both Perl and Unix shell script language are used in the programs of data processing and the programs of jobs controlling.

3.2 Distributed Computation

Up to 40 computers are used for the simulations. They are connected by a network for data communications. Each computer can simulate island formation with a unique set of simulation parameters. A controlling computer is used to launch the simulations, control the simulations and store the data. The simulation program is compiled and run using a script program. The commands for launching simulations are sent using the program "rsh". The graphic outputs are displayed on the controlling computer through the network.

X-window protocol is used for the graphic display. At the beginning of a simulation, the program reads the Green's function table and energy estimation table from the controlling computer and the results are saved to the controlling computer through the network using the network file system (NFS) protocol.

The simulation results are processed using script programs. The surfaces morphology, the energies, the surface roughnesses and other results are plotted. The graphs and tables of the results are then inserted into a hyper-text markup language (HTML) file, so that the results can be browsed by web browsers, such as Netscape Communicator. It is a useful and convenient method to read the large amount of simulation results generated from the many computers.

3.3 Graphic Interface

A graphic interface can instantly show a lot of information about the simulation, such as the surface configuration, the displacements of atoms, the strain and errors. This information can also help in debugging.

Graphic libraries called Mesa and GLUT are used. Mesa is an implementation of the graphic library OpenGL, and GLUT is a toolkit based on OpenGL. OpenGL is a standard graphic library in the computer industry, so our graphic interface modulus can directly port to most computer systems without modification. Figure 3.2 is the structure of the display system. We can see that the main program uses Mesa and GLUT to display graphics, and Mesa and GLUT use the X-window system and the library Xlib. With the X-window system, simulation programs display graphics on a controlling computer

through the network. Then, the simulations can be controlled and monitored through a single computer, the controlling computer.

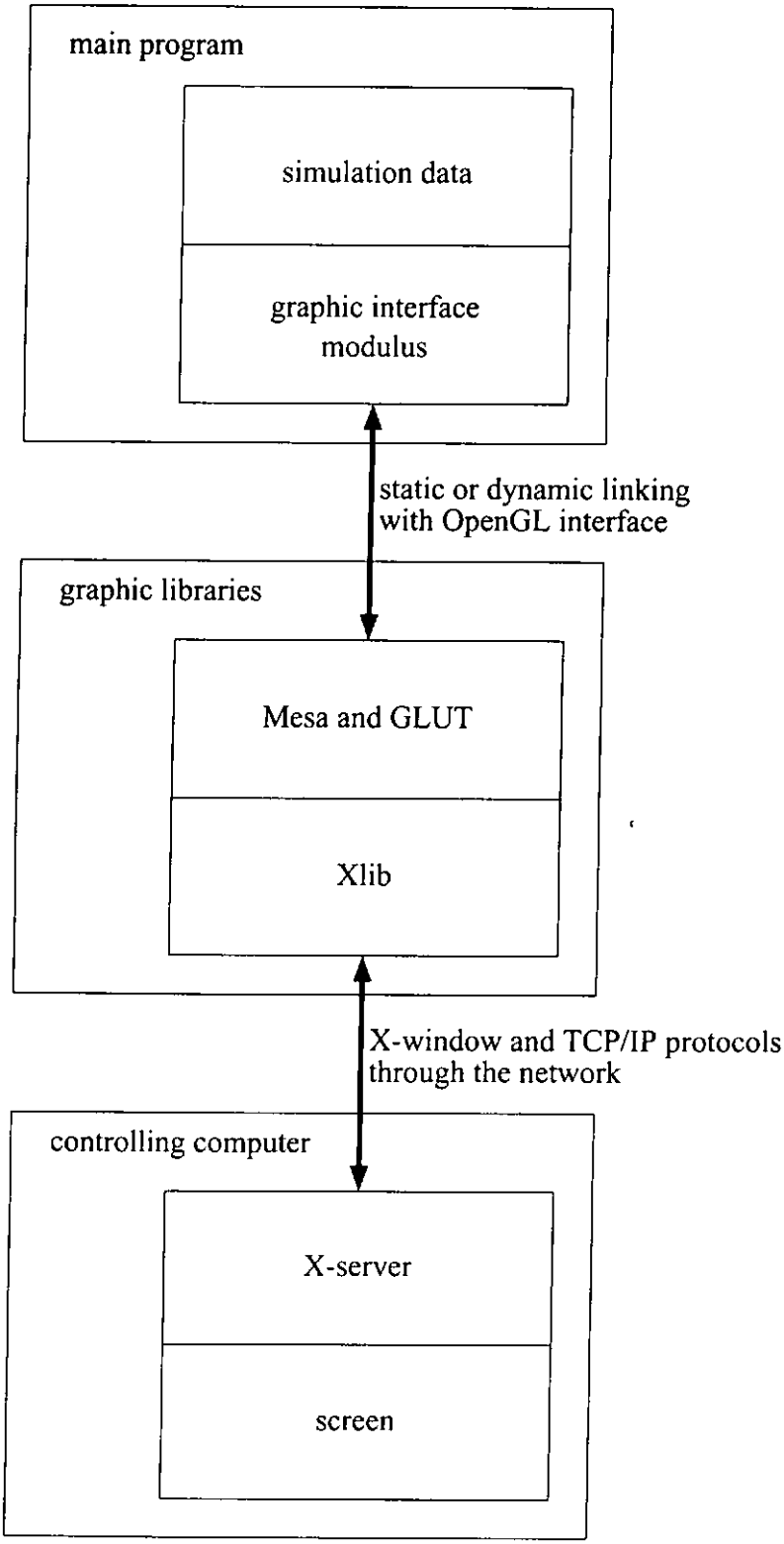

Figure 3.2: Structure of the display system. The main program and the program libraries are linked with OpenGL interface. Then, the graphic is sent to the controlling computer with X-window protocol and displayed on the screen of the controlling computer.

Chapter 4

Results

Island formation is simulated both under deposition and annealing conditions. In the simulation of annealing, the surface is initially flat and no new atom is deposited onto the surface. In simulation of deposition, new atoms will be added at random positions on the surface periodically.

Our model parameters are appropriate to the widely studied $Si_{1-x}Ge_x/Si$ system. The elastic constants for springs of nearest and next nearest neighboring atoms are $k_N = 1.878$ eV Å^{-2} and $k_{NN} = k_N/2$ respectively. This choice gives the correct modulus c_{11} of silicon and a shear modulus constant along tangential and diagonal directions. The ratio between k_N and k_{NN} provides equal Young's modulus in the tangential and diagonal directions, despite a slight anisotropy in the Young's modulus. We assume a substrate lattice constant $a_s = 2.7155$Å so that a_s^3 gives the correct atomic volume in crystalline silicon. The lattice constant a_f of the film material is related to the lattice misfit $\varepsilon = (a_f - a_s)/a_f$ which has a compositional dependence $\varepsilon = 0.04x$. The bond strength for both nearest and next nearest neighboring bonds is $\gamma_N = \gamma_{NN} = 0.4$ eV. The adatom

diffusion coefficient and the adatom hopping energy barrier are $D_0 = 5.2 \times 10^{13}$ Å^{2}s^{-1} and $E_a = 0.67$ eV respectively. This gives the appropriate adatom diffusion coefficient for Si(100). The substrate dimension is 1024 lattice spacings×1024 lattice spacings, which is limited by the computer resources. To speed up the simulations, we put the maximum hopping step size $s_{\max} = 8$ or 20 respectively for $x > 0.6$ or $x \leq 0.6$.

The parameter of the super-particle size is $r_0 = 3$. The typical error in ΔE_m is only about 10% of the variations in ΔE_m overall various sites on the surface. The surface morphology of the results are similar if r_0 is varied from 3 to 9.

4.1 Annealing

We have simulated annealing of initially flat films of 30 mono-layers (ML) at temperature $T = 1000$K.

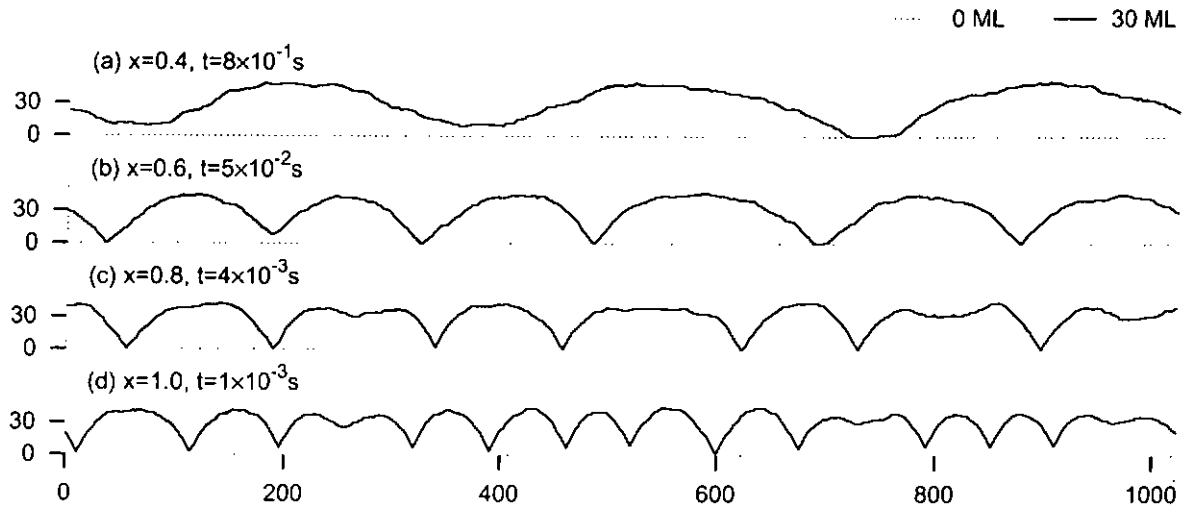

Figure 4.1: Snapshots of annealed films with (a) $x = 0.4$, (b) $x = 0.6$, (c) $x = 0.8$ and (d) $x = 1$. The horizontal lines indicate the interfaces between films and substrates..

Figure (4.1) shows the surface profiles after the islands are fully developed. The cusps on the surfaces are limited by either the substrate or the step height limit imposed in our

model. In the result for $x = 0.4$, we can clearly observe the ripples.

From this result, we find that the island size depends on the Ge concentration x, or the misfit $\varepsilon = 0.04x$. The higher the misfit, the smaller the islands. Applying Fast Fourier transformation on a surface, we find out the island size λ from the power spectra of 11 realizations of surfaces grown under identical conditions.

For example, averaging power spectra from 11 simulated $Si_{0.4}Ge_{0.6}$ films, we have the curve in figure 4.2. We can find a peak in the graph at wavelength 205 lattice spacings. The weighted average of the wavenumber of the data points in the peak is calculated and its wavelength is treated as the average island size λ. For this example of $Si_{0.4}Ge_{0.6}$ films, the average island size λ equals to 187 lattice spacings.

Figure 4.3 shows the average island size λ against the Ge concentration x in the film. In the figure, we obtain $\lambda \sim x^{-1.8}$ in reasonable agreement with x^{-2} from the ATG instability theory.

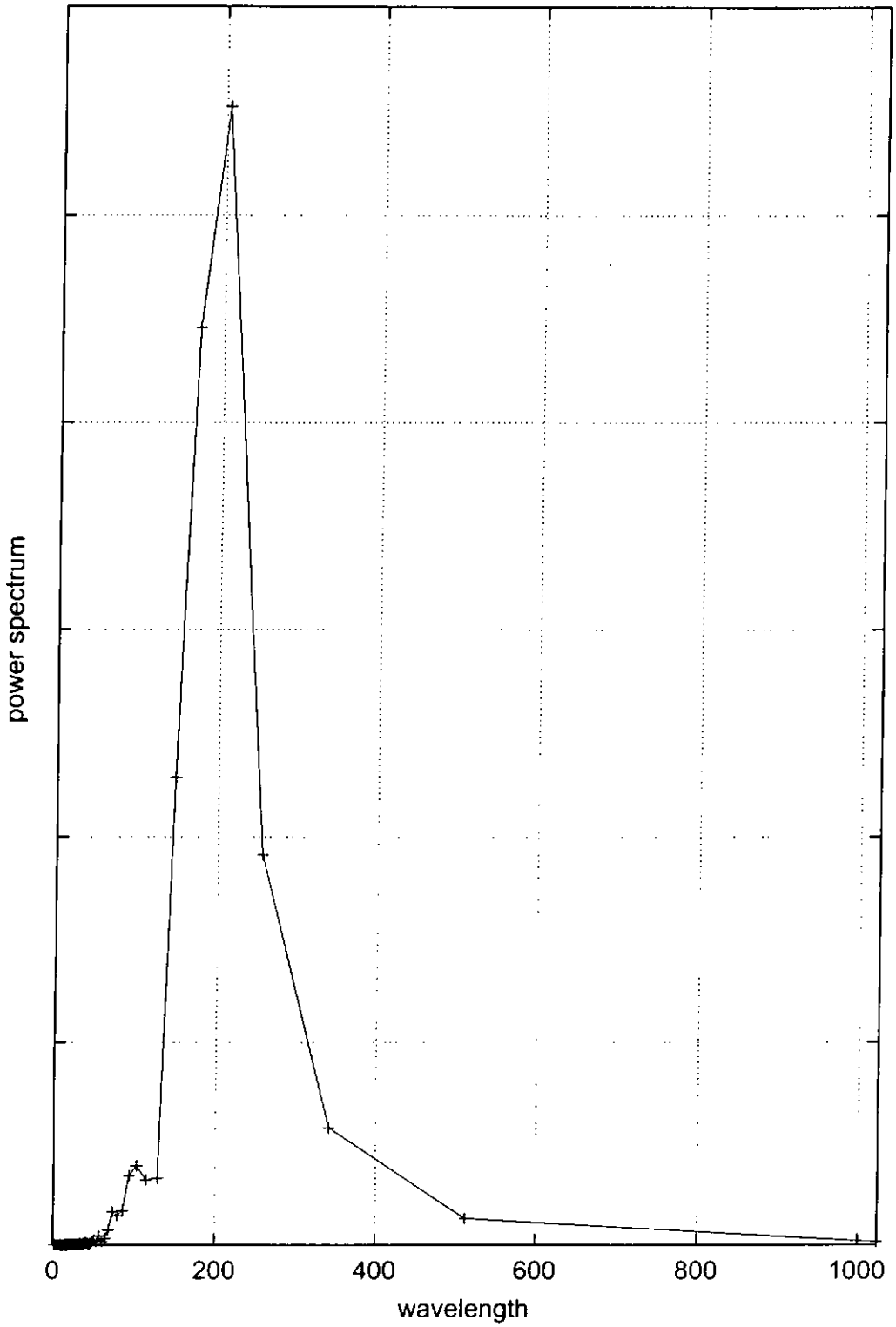

Figure 4.2: The averaged power spectrum from 11 simulated $Si_{0.4}Ge_{0.6}$ films.

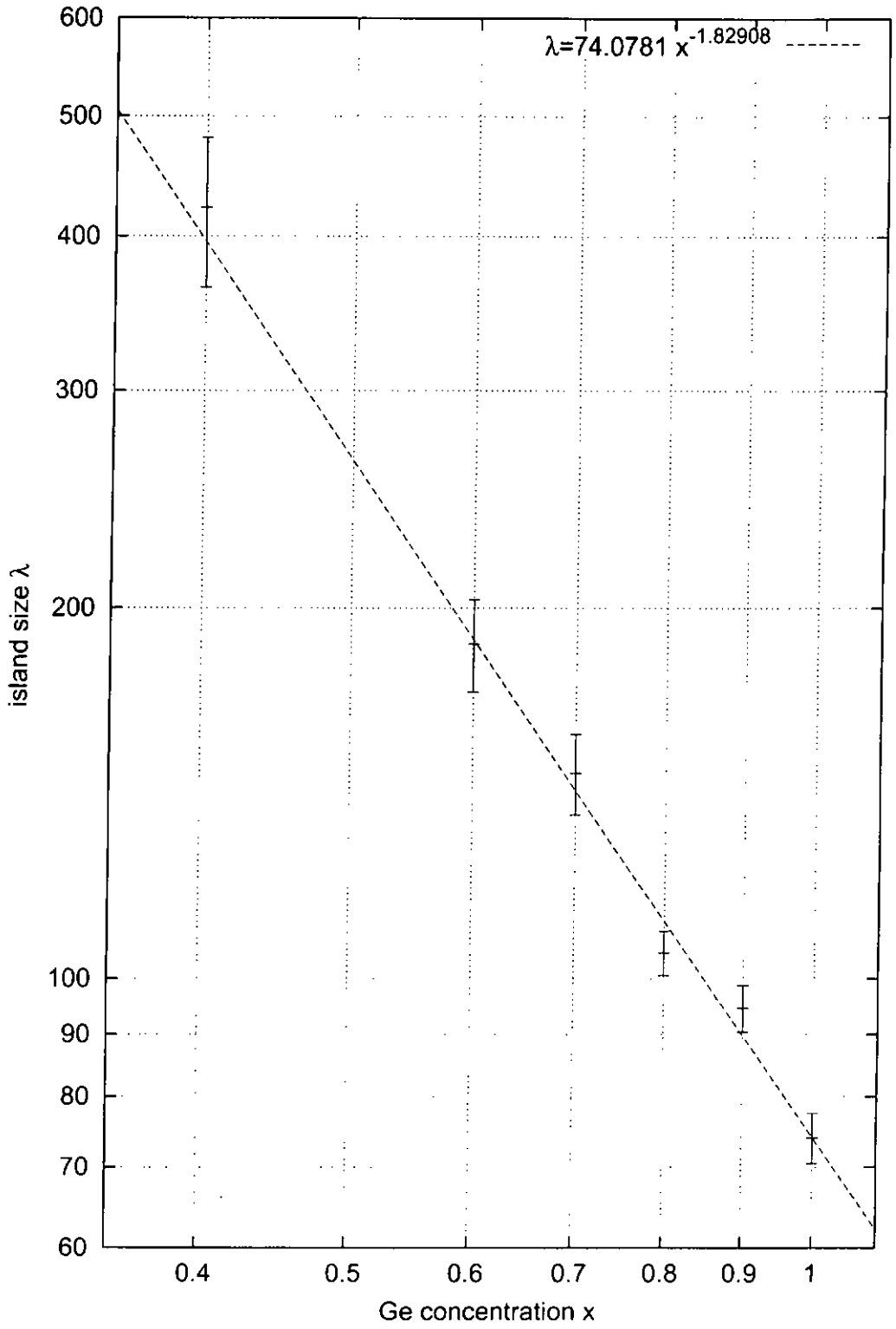

Figure 4.3: Island size λ against Ge concentration x. The relation $\lambda \sim x^{-1.8}$ is obtained.

4.2 Deposition

In the simulations of film growth with deposition, an atom is deposited onto a random column after every time period τ. For a lattice of width L in unit of lattice spacings and a deposition rate Φ in mono-layers per second (ML s^{-1}), the time period τ can be calculated from the equation $\tau = L/\Phi$.

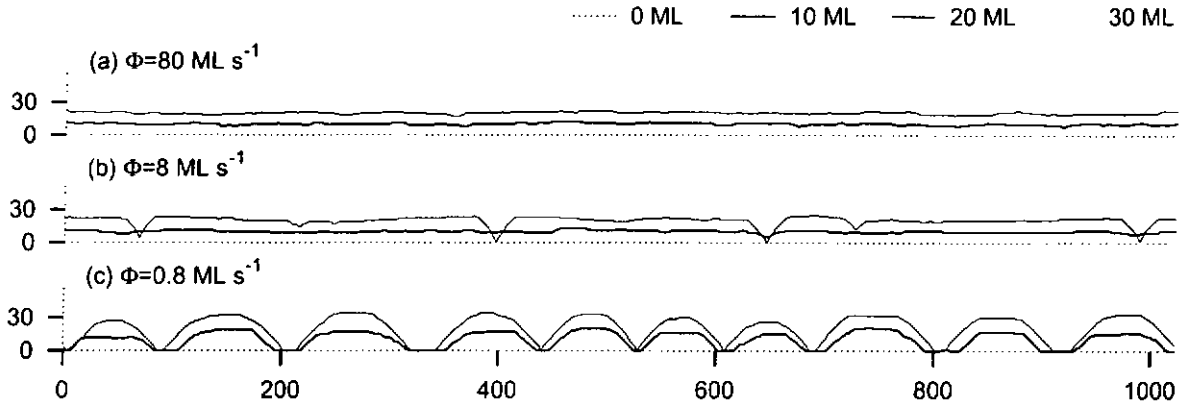

Figure 4.4: Snapshots of film growth at temperature T=600K, pure Ge film. The deposition rates Φ are (a) 80, (b) 8, and (c) 0.8 mono-layers per second.

Figure (4.4) shows the results of the deposition of pure Ge films (i.e. $x = 1$) with misfit $\varepsilon = 4\%$ at temperature $T = 600$K. At very high deposition rate $\Phi = 80$ ML s^{-1} (figure 4.4a), we observe layer-by-layer growth. At slower deposition rate $\Phi = 8$ ML s^{-1} (figure 4.4b), the film is initially flat but pits then develop. A detailed examination of the morphological evolution indicates that the pits appear rather independently and suddenly. Once created, they are immediately bounded by side-walls at an energetically favorable 45°inclination. These features strongly support the nucleation mechanism for their formation. Note that pits are energetically more favorable than islands [Tersoff, 1994]. At $\Phi = 0.8$ ML s^{-1} (figure 4.4c), islands with 45°side-walls nucleate at very early stage before the film is sufficiently thick for pit formation. Further decreasing the deposition rate

leads to similar but more widely separated islands.

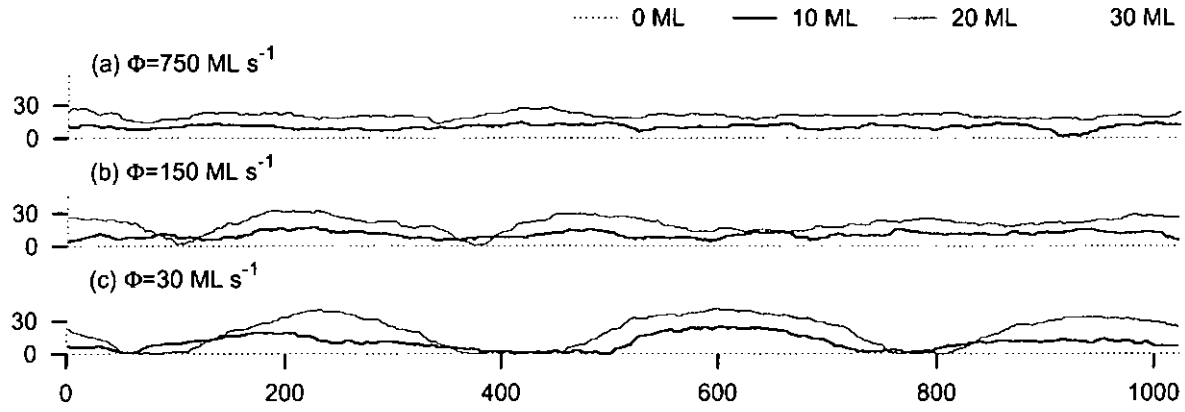

Figure 4.5: Snapshots of film growth at temperature T=1000K, $Si_{0.5}Ge_{0.5}$ film. The deposition rates Φ are (a) 750, (b) 150, and (c) 30 mono-layers per second.

Figure (4.5) shows the results of the deposition of $Si_{0.5}Ge_{0.5}$ films on Si substrates with $\varepsilon = 2\%$ at $T = 1000$K. Depending on Φ, we observe analogous layer-by-layer growth (figure 4.5a), layer-by-layer growth followed by roughening (figure 4.5b), and island growth (figure 4.5c). However, the islands in figures 4.5b and 4.5c emerge gradually from ripple-like perturbations with local surface inclinations increasing steadily and relatively synchronously in agreement with experiments [Floro *et al.*, 1999; Tromp *et al.*, 2000] and ATG instability theory. This regime has not been reported in previous atomistic simulations mainly due to inaccuracies in accounting for the long-range parts of the elastic interactions or the rather thin substrates used [Orr, *et al.*, 1992; Barabási, 1997; Khor, 2000].

At low misfit and high temperature, we observe ripples and subsequently gradual island formation consistent with the ATG instability theory. At high misfit and low temperature, islands or pits are generated via the nucleation pathway. These suggest a non-trivial competition between roughening mechanisms, although reliable quantitative determination of the crossover conditions is beyond the scope of our model. The ATG instability is

the most promising description of island formation in $Si_{1-x}Ge_x$ films at low, and probably also at high lattice misfit [Floro *et al.*, 1999; Vailionis *et al.*, 2000]. However, the nucleation mechanism applied to high misfit regimes in certain experimental situations has not been ruled out [Kästner, 1999]. Thus the competition of mechanisms can be important for interpreting experimental results.

In our simulations, for deposition rates close to the relevant roughening rate, kinetically limited wetting layers develop prior to roughening. At lower deposition rates, islands form at an early stage and are more widely separated. This may be related to the great variation in how closely the islands are packed under various conditions in experiments [Floro *et al.*, 1999; Vailionis *et al.*, 2000].

Chapter 5

Conclusions

The accelerated algorithms described in chapter 2 greatly improve the computational performance of the simulations. They properly and efficiently account for the long range elastic interactions. The simulation can run with a large lattice of dimensions up to 1024×1024. About 10^8 atomic hoppings are involved within one day on a 2GHz desktop computer. Long range elastic interactions and a large lattice provide the necessary conditions for simulating ripple growth. With these fast algorithms, we simulate annealing and deposition of strained heteroepitaxial layers. In the simulation of annealing, the relation between the island size and the misfit agrees with the instability theory. The roughening by ripples is mainly due to the ATG instability.

By controlling the growing conditions, we can simulate ripples and subsequently gradual island formation consistent with the ATG instability theory. We can also simulate islands or pits generated via the nucleation pathway. These suggest a non-trivial competition between roughening mechanisms and can be important for interpreting experimental results. The three growth modes, Frank-van der Merwe growth, Volmer-Weber growth

and Stranski-Krastanow growth, can be simulated by controlling the deposition rate.

References

Asaro, R. J. and Tiller, W. A. "Interface morphology development during stress corrosion cracking". *Metallurgical Transactions A*, Vol. 3, pp. 1789 (1972).

Barabási, A.-L. "Self-assembled island formation in heteroepitaxial growth". *Applied Physics Letters*, Vol 70, pp. 2565 (1997).

Eaglesham, D. J. and Cerullo, M. "Dislocation-Free Stranski-Krastanow Growth of Ge on Si(100)". *Physical Review Letters*, Vol. 64, pp. 1943-1496 (1990).

Frank, F. C. and van der Merwe, J. H., *Proc. R. Soc. Landon, Ser. A*, Vol. 198, pp. 205 (1949).

Floro, J. A., Chason, E., Twesten, R. D., Hwang, R. Q. and Freund, L. B. "SiGe Coherent Islanding and Stress Relaxation in the High Mobility Regime". *Physical Review Letters*, Vol. 79, pp. 3946-3949 (1997).

Floro, J. A., Chason, E., Freund, L. B., Twesten, R. D., Hwang, R. Q and Lucadamo, G. A. "Evolution of coherent islands in $Si_{x-1}Ge_x$/Si(001)". *Physical Review B*, Vol. 59, pp. 1990-1998 (1999).

Grinfeld, M. A. "Instability of the separation boundary between a non-hydrostatically stressed elastic body and a melt". *Soviet Physics Doklady*, Vol. 31, pp. 831-834 (1986).

Kamins, T. I., Carr, E. C., Williams, R. S. and Rosner, S. J. "Deposition of three-dimensional Ge islands on Si(001) by chemical vapor deposition at atmospheric and reduced pressures". *Journal of Applied Physics*, Vol. 81, pp. 211-219 (1997).

Kästner, M. and Voigtländer, B. "Kinetically Self-Limiting Growth of Ge Islands on Si(001)". *Physical Review Letters*, Vol. 82, pp. 2745-2748.

Khor, K. E. and Das Sarma, S. "Quantum dot self-assembly in growth of strained-layer thin films: A kinetic Monte Carlo study". *Physical Review B*, Vol. 62, pp. 16657-16664 (2000).

Medeiros-Ribeiro, G., Bratkovski, A. M., Kamins, T. I., Ohlberg, D. A. A. and Williams, R. S. "Shape Transition of Germanium Nanocrystals on a Silicon (001) Surface from Pyramids to Domes". *Science*, Vol. 279, pp. 353-355 (1998).

Meixner, M., Schöll, E., Shchukin, V. A. and Bimberg, D. "Self-Assembled Quantum Dots: Crossover from Kinetically Controlled to Thermodynamically Limited Growth". *Physical Review Letters*, Vol. 87, article 236101 (2001).

Mo, Y.-W., Savage, D. E., Swartzentruber, B. S. and Lagally, M. G. "Kinetic Pathway in Stranski-Krastanov Growth of Ge on Si(001)". *Physical Review letters*, Vol. 65, pp. 1020-1023 (1990).

Orr, B. G., Kessler, D., Snyder, C. W. and Sander, L. "A Model for Strain-Induced Roughening and Coherent Island Growth", *Europhysics Letters*, Vol. 19(1), pp. 33-38 (1992).

Pidduck, A. J., Robbins, D. J., Cullis, A. G., Leong, W. Y. and Pitt, A. M. "Evolution of surface morphology and strain during SiGe epitaxy", *Thin Solid Films*, Vol. 222, pp. 78-84 (1992).

Press, W. H., Teukolsky, S. A., Vetterling, W. T. and Flannery, B. P. "Conjugate Gradient Method for a Sparse System". *Numerical Recipes in C*, Cambridge University Press, USA, pp.83-89 (1992).

Ratsch, C., Zangwill, A. and Šmilauer, P. "Scaling of heteroepitaxial island sizes". *Surface Science*, Vol. 314, pp. L937-L942 (1994).

Ross, F. M., Tromp, R. M. and Reuter, M. C. "Transition States Between Pyramids and domes During Ge/Si Island Growth". *Science*, Vol 286, pp. 1931-1934 (1999).

Srolovitz, D. J., "ON THE STABILITY OF SURFACES OF STRESSED SOLIDS". *Acta metallurgica*, Vol. 37, pp. 621-625 (1989).

Stranski, I. N. and Von Krastanow, L., *Sitz. Ber. Akad. Wiss. Let. Mainz Math.-Natur.*, Vol. 146, pp. 797 (1939).

Sutter, P. and Lagally, M. G. "Nucleationless Three-Dimensional Island Formation in Low-Misfit Heteroepitaxy", *Physical Review Letters*, Vol. 84, pp. 4637-4640 (2000).

Tersoff, J. and LeGoues, F. K. "Competing Relaxation Mechanisms in Strained Layers", *Physical Review Letters*, Vol 70, pp. 2782-2785 (1994).

Tomitori, M., Watanabe, K., Kobayashi, M. and Nishikawa, O. "STM study of the Ge growth mode on Si(001) substrates". *Applied Surface Science*, Vol. 76/77, pp. 322-328 (1994).

Tromp, R. M., Ross, F. M. and Reuter, M. C. "Instability-Driven SiGe Island Growth". *Physical Review Letters*, Vol. 84, pp. 4641-4644 (2000).

Vailionis, A., Cho, B., Glass, G., Desjardins, P., Cahill, D. G. and Greene, J. E. "Pathway for the Strain-Driven Two-Dimensional to Three-Dimensional Transition during Growth of Ge on Si(001)". *Physical Review Letters*, Vol 85, pp. 3672-3675 (2000).

Volmer, M. and Weber, A., *Z. Phys. Chem.*, Vol. 119, pp. 277 (1926).

Windisch, D. and Becker, P. "Silicon Lattice Parameters as an Absolute Scale of Length for High Precision Measurements of Fundamental Constants". *Physica Status Solidi A*, Vol. 118, pp. 379-388 (1990).